Topological phase transition in the archetypal f-electron correlated system of cerium

Junwon Kim,[1,*] Dong-Choon Ryu,[1,*] Chang-Jong Kang,[1,†] Kyoo Kim,[1,2] Hongchul Choi,[1,‡] T.-S. Nam,[1] and B. I. Min[1,§]
[1]*Department of Physics, Pohang University of Science and Technology, Pohang 37673, Korea*
[2]*MPPHC_CPM, Pohang University of Science and Technology, Pohang 37673, Korea*

(Received 14 June 2019; revised manuscript received 22 September 2019; published 25 November 2019)

A typical f-electron Kondo lattice system Ce exhibits a well-known isostructural transition, the so-called γ-α transition, accompanied by an enormous volume collapse. Most interestingly, we have discovered that a topological phase transition also takes place in elemental Ce, concurrently with the γ-α transition. Based on the dynamical mean-field theory approach combined with density functional theory, we have unraveled that the nontrivial topology in α-Ce is driven by the f-d band inversion, which arises from the formation of a coherent $4f$ band around the Fermi level. We captured the formation of the $4f$ quasiparticle band that is responsible for the Lifshitz transition and the nontrivial Z_2 topology establishment across the phase boundary. This discovery provides a concept of a "topology switch" for topological Kondo systems. The "on" and "off" switching knob in Ce is versatile in a sense that it is controlled by the available pressure ($\lesssim$1 GPa) at room temperature.

DOI: 10.1103/PhysRevB.100.195138

The physics of strongly correlated f-electron materials has been a longstanding subject of special interest due to the complex interplay between the underlying interactions, such as strong Coulomb correlations, spin-orbit (SO) coupling, and the hybridization of the localized f and conduction electrons. More intriguing is that the interplay is very sensitive to small changes in the external parameters. Elemental Ce, which has one occupied f electron in its atomic phase, is a prototypical f-electron Kondo lattice system exhibiting such sensitivity. Indeed, Ce shows a rich phase diagram (see Fig. 1) and many interesting physical properties as a function of temperature (T) and pressure (P) [1–4]. The first-order isostructural volume collapse transition from the γ to α phase of face-centered-cubic (fcc) Ce is the most representative phenomenon that experiences the sensitivity. However, the driving mechanism of the γ-α transition is still under debate, between the two well-known models: the Mott transition [5] versus Kondo volume collapse [6]. The current consensus is that there exists at least a significant change in the Kondo hybridization between the localized $4f$ electrons and conducting electrons across the transition [7–10]. This peculiarity in Ce could facilitate the emergence of nontrivial topology in the ground-state α phase of Ce.

In a recent theoretical work on topological Kondo insulators [11], it is shown that the Kondo hybridization in f-electron systems can play an important role in the formation of nontrivial topology. Since then, many subsequent studies have been reported to search for nontrivial topological materials, where the Kondo hybridization gap exists, e.g., CeNiSn, $CeRu_4Sn_6$, $Ce_3Bi_4Pt_3$, SmB_6, SmS, and YbB_{12} [11–17]. Despite extensive studies, however, the topological nature of mother elements, Ce, Sm, and Yb, supplying the correlated f electrons to the above Kondo insulator compounds, has not been explored yet. Here, we report, based on the dynamical mean-field theory (DMFT) approach combined with density functional theory (DFT) that has been successful in describing the electronic structures of Ce and Ce compounds [8,9,18,19], that a narrow f-band metal α-Ce has the nontrivial topology of a topological-insulator (TI)-type and topological-crystalline-insulator (TCI)-type nature, and the topological phase transition and the Lifshitz electronic transition occur concomitantly with the γ-α volume collapse transition in Ce.

Figure 2 shows the DMFT band structures and the densities of states (DOS) of γ- and α-Ce. In the DMFT calculations, we have used the Coulomb correlation (U) and the exchange (J) interaction parameters of $U = 5.5$ eV and $J = 0.68$ eV for the Ce f electrons (refer to the Supplemental Material for the computational details [21]). The $4f$ spectral weights of both phases have three main parts in common: the lower Hubbard band (LHB) at -2.0 to -2.5 eV corresponding to the $4f^0$ final state, the upper Hubbard band (UHB) at 2–4 eV corresponding to the $4f^2$ final state, and the Kondo resonances near the Fermi level (E_F) corresponding to the $4f^1$ final states. The energy positions of LHB and UHB are in good agreement with photoemission spectroscopy (PES) [22–25] and inverse PES experiments [26]. One of the most notable features in Fig. 2 is that the spectral weight of the Kondo resonance around E_F is much stronger in α-Ce than in γ-Ce, and exhibits the coherent quasiparticle band feature in α-Ce, as is consistent with previous PES [22–26] and theoretical reports [27–30]. As will be discussed below, these contrasting Kondo resonance features between the two phases lead to quite different topological classes: trivial and nontrivial Z_2 topologies for γ-Ce and α-Ce, respectively.

*These authors contributed equally to this work.
†Present address: Department of Physics and Astronomy, Rutgers University, Piscataway, New Jersey 08854, USA.
‡Present address: IBS-CCES, Seoul National University, Seoul 08826, Korea.
§bimin@postech.ac.kr

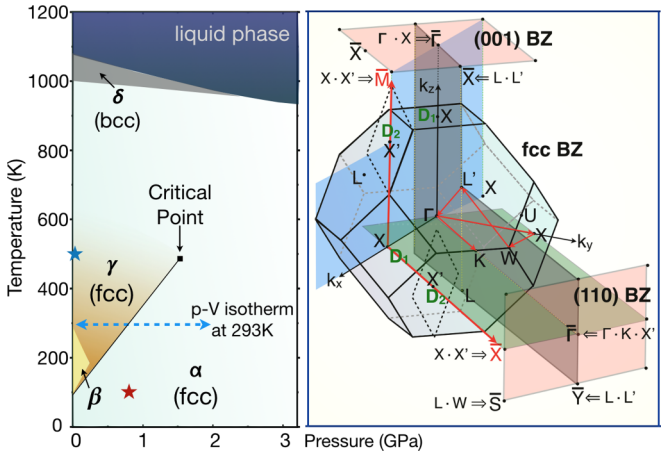

FIG. 1. Left: A phase diagram of Ce [20] (see also the Supplement Material [21]). α-Ce at the red star and γ-Ce at the blue star are selected for a comparison of electronic structures in Fig. 2. The blue dotted line corresponds to the P-V isotherm at 293 K. Right: The bulk BZ of fcc Ce and its (001) and (110) surface BZ. There are two independent mirror planes of $k_y = 0$ (in blue) and $k_x = k_y$ (in gray), which, respectively, yield two mirror-symmetry lines along $\bar{M}$-$\bar{\Gamma}$-$\bar{M}$ and $\bar{X}$-$\bar{\Gamma}$-$\bar{X}$ in the (001) surface BZ. Similarly, in the (110) surface BZ, two mirror-symmetry lines are formed along $\bar{Y}$-$\bar{\Gamma}$-$\bar{Y}$ and $\bar{X}$-$\bar{\Gamma}$-$\bar{X}$.

The incoherent and coherent $4f$ spectral weights for γ-Ce and α-Ce, respectively, are more clearly shown in the amplified DMFT band structures in Fig. 3. It is seen in Fig. 3(a) that, for γ-Ce, $4f$ electrons are incoherent, and so mainly the $5d$ band crosses E_F, which agrees well with the optical spectroscopy result [31]. In contrast, for α-Ce, the coherent $4f$ quasiparticle band feature is evident near E_F in Fig. 3(b), which is the origin of the effective mass enhancement of charge carriers and the change of the charge carrier character from $5d$ to $4f$. The coherent band feature for α-Ce is corroborated by the fact that the DMFT bands have almost the same dispersion as the renormalized DFT bands rescaled approximately by $1/2$ [dotted green line in Fig. 3(b)].

The different electronic structures between the two phases are also reflected in the Fermi surfaces (FSs). The shapes of FSs in Fig. 3(d) are topologically different, suggesting that the γ-α transition corresponds to the Lifshitz transition (see the Supplemental Material [21]). It is noteworthy in Fig. 3(d) that, while the DMFT FS of γ-Ce is very close to that obtained from the DFT-OPENCORE ("$4f$-OPENCORE") calculation considering the $4f$ electrons as core electrons, the DMFT FS of α-Ce is quite similar to the DFT FS. These results indicate that, for γ-Ce, the contribution of $4f$ electrons to the FS is negligible, and, for α-Ce, the $4f$ quasiparticle band at E_F can be described properly by the DFT band (see Fig. S1 of the Supplemental Material [21]).

The key ingredient that makes the difference has something to do with the degree of the renormalization factor (quasiparticle weight) Z, arising from the Coulomb correlation interaction of $4f$ electrons. The renormalization factor Z is obtained from the self-energy $\Sigma(i\omega_n)$ at the lowest Matsubara frequency. As shown in Fig. S5 of the Supplemental Material [21], we have obtained qualitatively different behaviors of $\Sigma(\omega)$'s between the α and γ phases, which produce quite distinct electronic structures and resulting physical parameters. Indeed, Fig. 3(e) shows that Z increases discontinuously across the γ-α transition. As a result, both the hybridization strength $\Delta(\omega)$ [Fig. 3(c)] and the f-f hopping strength, which are to be effectively proportional to Z, are enhanced for α-Ce, which give rise to the enhanced $4f$ spectral weight and help to form the coherent $4f$ band around E_F [29].

The evolution of the electronic structure across the γ-α transition makes the elemental Ce more interesting in a topological sense. The coherent quasiparticle band in α-Ce, which, via the hybridization with the conduction band, brings about

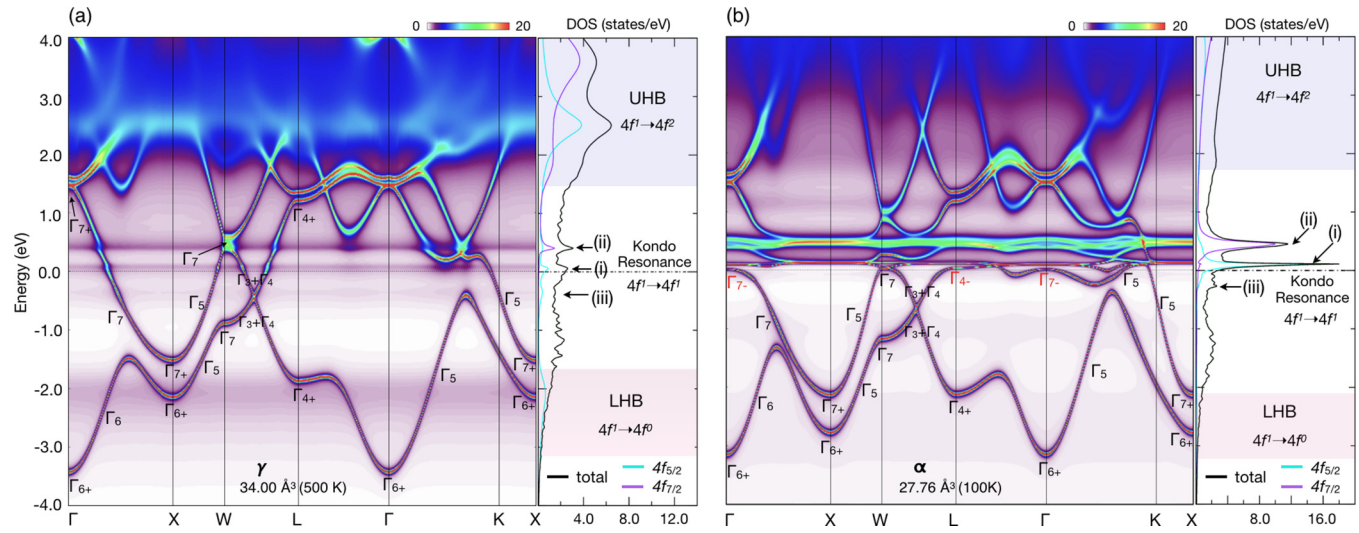

FIG. 2. (a) The DMFT electronic structure and DOS for γ-Ce calculated at $V = 34$ Å^3 ($P =$ ambient pressure) and $T = 500$ K, and (b) those for α-Ce calculated at $V = 27.76$ Å^3 ($P = 0.88$ GPa) and $T = 100$ K. The $4f$ spectral weights of both phases consist of mainly three parts: UHB at 2–4 eV, LHB at -2.0 to -2.5 eV, and the Kondo resonance near E_F. In addition to the Kondo resonance near E_F (i), the SO side peaks (ii) and (iii) are seen at $\sim \pm 0.3$ eV. Note that only α-Ce shows the coherent quasiparticle $4f$ band around E_F, which is shown more clearly in Fig. 3.

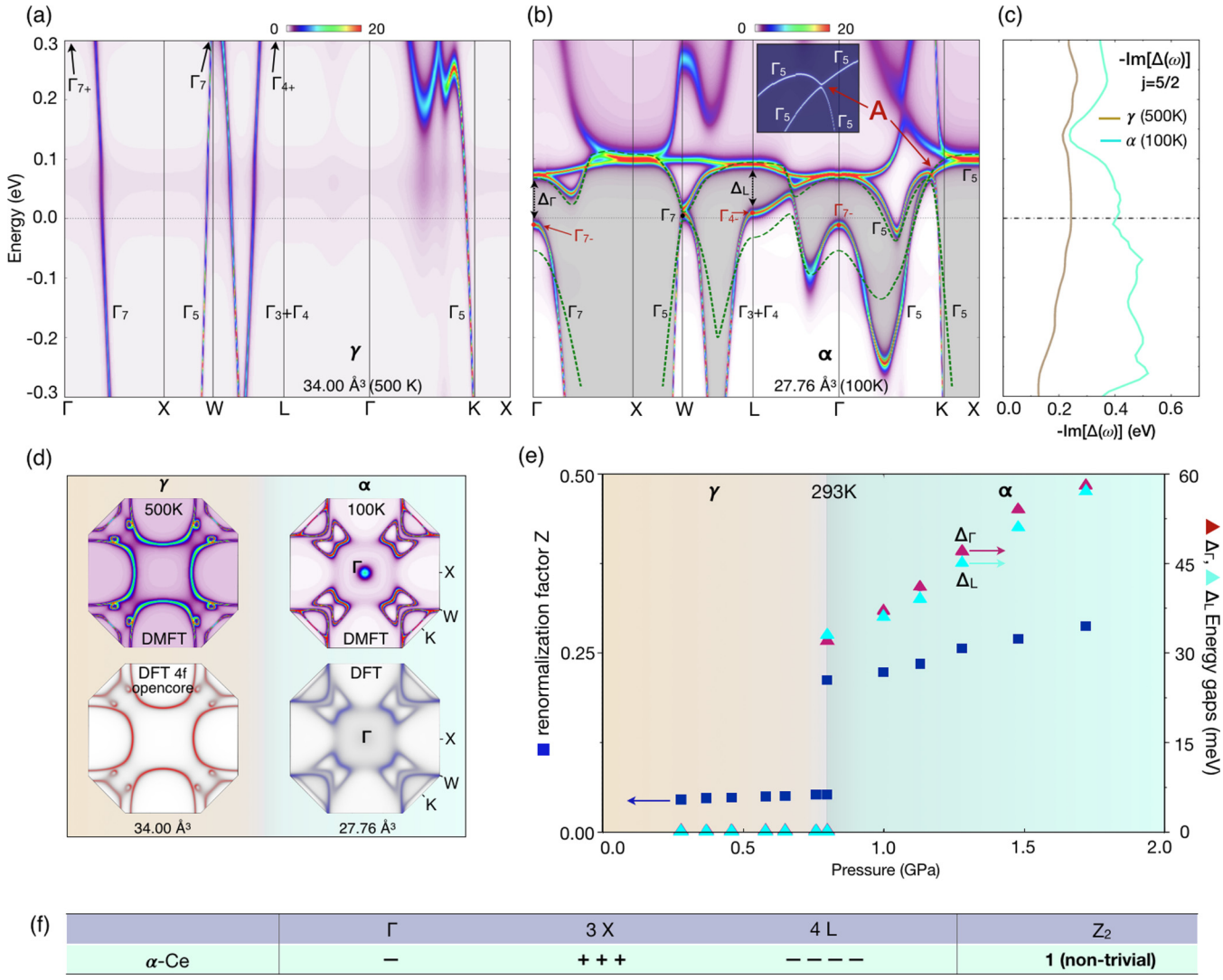

(f)

	Γ	3 X	4 L	Z_2
α-Ce	−	+ + +	− − − −	**1 (non-trivial)**

FIG. 3. The amplified DMFT electronic structures near E_F: (a) for γ-Ce and (b) for α-Ce. For γ-Ce, $4f$ states are hardly seen, because they are incoherent. For α-Ce, the coherent $4f$ bands formed around E_F produce, via the hybridization with the conduction band, the separated bands with the gap in-between (colored in gray). There exist clear energy gaps at the TRIM points of Γ, X and L, and also small energy gaps at W, in between L-Γ, and at A along Γ-K. The inset shows the gap formation at A, arising from the same Γ_5 symmetry of the crossing bands [32]. The green dotted lines overlaid with DMFT bands are the DFT bands rescaled by 1/2. (c) Imaginary part of the DMFT hybridization function $\Delta(\omega)$. (d) DMFT and DFT FSs for both phases (see also Fig. S1 [21]). (e) The renormalization factor Z and the energy gaps at Γ and L (Δ_Γ and Δ_L) are displayed as a function of pressure (see also Figs. S2–S4 [21]). The first-order-type phase transition is manifested across the γ-α transition. (f) The product of the parity eigenvalues of α-Ce at eight TRIM points in the fcc BZ.

the hybridization gap in the α-Ce phase, is indicated by the gray-shaded area in Fig. 3(b). The energy gaps are clearly seen at every time-reversal invariant momentum (TRIM) point of Γ, X, and L, while those at W and in between L-Γ are barely gapped. Then, with respect to the hybridization gap, the $5d$ band of even parity and the $4f$ band of odd parity are inverted at the TRIM point X. Since the crystal structure is symmetric under the inversion operation, the additional odd parity to the TRIM points yields the nontrivial Z_2 topology of α-Ce, as shown in Fig. 3(f).

Figure 3(e) shows that the necessary conditions for the nontrivial Z_2 topology, the buildup of the coherent $4f$ band and the opening of the hybridization gap, are established at the very starting edge (pressure 0.8 GPa at 293 K) of the α phase in the γ-α transition. Note that no gaps are present in the γ phase, but the gaps at the TRIM points, Δ_Γ and Δ_L of about 30 meV ($\Delta_X > 2$ eV), are suddenly developed in the α phase. This implies that the first-order topological phase transition would occur concomitantly with the γ to α volume collapse transition. A more detailed evolution of the band structures across the γ-α transition is given along a P-V isotherm at 293 K in Fig. S2 of the Supplemental Material. For comparison, the crossover-type topological phase transition, which is expected to occur above the critical point, is also discussed in the Supplemental Material [21].

In order to confirm the nontrivial Z_2 topological invariance of α-Ce, we have performed the surface electronic structure calculations for the slab geometry of α-Ce with a (001)

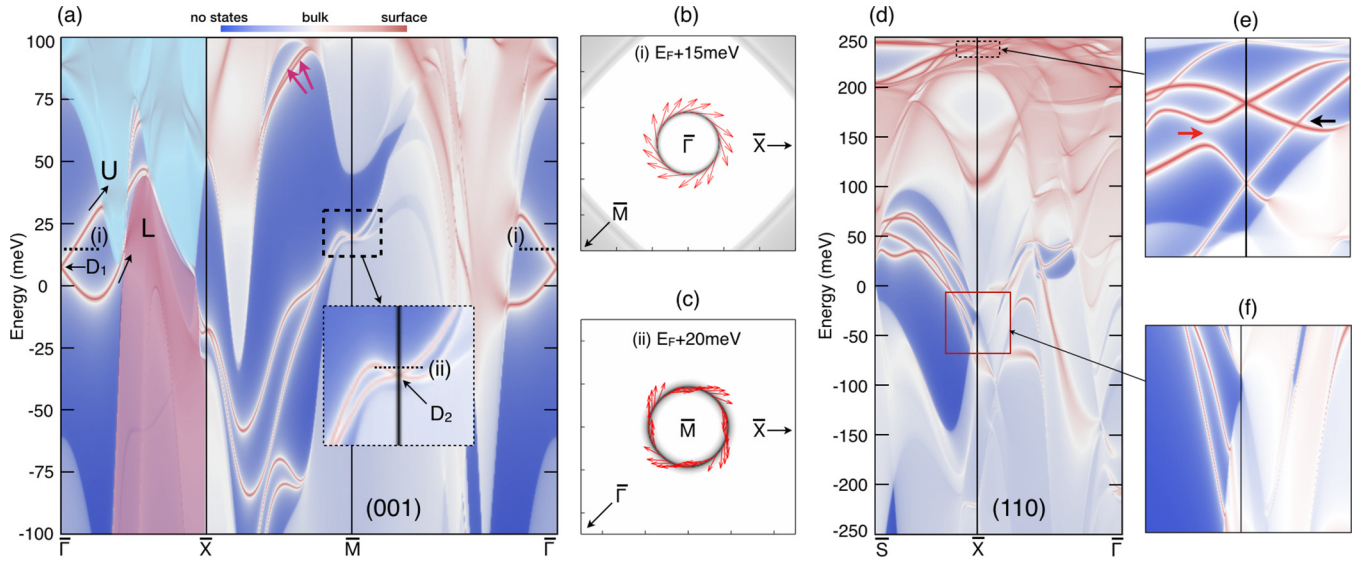

FIG. 4. (a) The (001) surface electronic structure of α-Ce, calculated by the tight-binding (TB) model with semi-infinite slabs. The TB Hamiltonian is constructed from the DFT band result (rescaled by $1/2$ near E_F). D_1: a Dirac point at $\bar{\Gamma}$; D_2: a Dirac point at $\bar{M}$; U: projected bulk bands above the indirect gap (cyan colored); L: projected bulk bands below the indirect gap (violet colored). (b), (c) The helical spin structures of the D_1 and D_2 Dirac cone energy surfaces, as indicated by (i) and (ii), respectively. (d) The (110) surface electronic structure of α-Ce. (e), (f) Amplified band structures inside the green square and the red square in (d), respectively. In (e), TSSs of a typical TCI-type nature are revealed with the gapped (red arrow) and protected (black arrow) Dirac points, while in (f), TSSs are mostly buried under the projected bulk bands.

surface and explored the existence of topological surface states (TSSs) in Fig. 4(a). Note that, as shown in Fig. 1, one X point is projected onto $\bar{\Gamma}$, while two nonequivalent X and X' points are projected onto $\bar{M}$ of the (001) surface BZ. Indeed, as shown in Fig. 4(a), the TSSs and corresponding Dirac points emerge in the indirect gap region at $\bar{\Gamma}$ (D_1) and $\bar{M}$ (D_2). Due to the bulk metallic nature of α-Ce, most parts of the Dirac bands at $\bar{M}$ are buried under the projected bulk bands and so the band connectivity is not clear. Nevertheless, it is evident in Fig. 4(a) that the surface states along $\bar{\Gamma}$-$\bar{X}$ are the Dirac cone states, because the lower surface band reaches the projected bulk bands (L) below the indirect gap, while the upper one reaches the projected bulk bands (U) above the indirect gap. The helical spin textures of the corresponding Dirac cone FSs around $\bar{\Gamma}$ and $\bar{M}$ in Figs. 4(b) and 4(c) also manifest the spin-momentum locking behavior, reflecting its topological nature.

The double Dirac points, which are supposed to be at $\bar{M}$ due to the projection of two nonequivalent X TRIM points (Fig. 1), are to be separated due to the hybridization between the bands of the double Dirac cones. On the (001) surface Brillouin zone (BZ) of α-Ce, there are two mirror-symmetric lines, $\bar{\Gamma}$-$\bar{X}$ and $\bar{\Gamma}$-$\bar{M}$, as shown in Fig. 1, which could play a key role in realizing the TCI-type nature. It is thus obvious that the band crossing along $\bar{X}$-$\bar{M}$ that is not a mirror-symmetric line would be gapped, but that along $\bar{M}$-$\bar{\Gamma}$ needs further consideration. However, the surface states along $\bar{M}$-$\bar{\Gamma}$ are completely buried under the projected bulk bands, and so it is not easy to identify the specific TCI-type band feature in Fig. 4(a). In view of the surface states inside the dotted black square and those along $\bar{X}$-$\bar{M}$ designated by the red arrows in Fig. 4(a), we just conjecture that the band crossing along $\bar{M}$-$\bar{\Gamma}$ would be gapped to have Rashba-type surface states, as reported for the golden phase of SmS (g-SmS) that is expected to have the same topological symmetry as α-Ce [33]. In fact, α-Ce is found to have the same mirror Chern numbers as g-SmS [34], as shown in Fig. S6 of the Supplemental Material [21].

We have also examined the TSSs for the (110) and (111) surfaces of α-Ce. For the (110) surface, single and double Dirac points are expected to be located at $\bar{\Gamma}$ and $\bar{X}$, respectively, as shown in Fig. 1. For the (111) surface, only the single Dirac point is expected at $\bar{M}$, as shown in Fig. S7 of the Supplemental Material [21]. As shown in Fig. 4(d) and Fig. S7, however, neither the (110) nor (111) surface states show a clear TI-type or TCI-type signature in the hybridization gap region, because, here too, most of the surface states near E_F are buried under the projected bulk bands. In this circumstance, for the (110) surface, one apparent TCI signature is seen at $\bar{X}$ near 240 meV in Fig. 4(e), which demonstrated the gapped and protected Dirac points along $\bar{X}$-$\bar{S}$ (red arrow) and $\bar{X}$-$\bar{\Gamma}$ (black arrow), respectively. This suggests that the near-E_F TSSs buried under the projected bulk bands in Fig. 4(f) would also have the TCI-type band nature.

Our finding highlights that a typical narrow f-band metal α-Ce is a topological Kondo system of TI- and TCI-type nature, and the "on" and "off" topology switch can be operative by using a P-tuning or T-tuning knob, accompanied by a first-order volume collapse and Lifshitz transitions. So Ce would be an excellent test bed for investigating the topological phase transition in f-electron Kondo lattice systems. It is thus highly desirable to explore the topological surface states in α-Ce, preferentially for its (001) surface, by using high-resolution angle-resolved PES measurements.

We would like to thank J. D. Denlinger, J.-S. Kang, and J. H. Shim for helpful discussions. This work was supported by the NRF (Grants No. 2017R1A2B4005175, No. 2018R1A6A3A01013431, and No. 2016R1D1A1B02008461), Max-Plank POSTECH/KOREA Research Initiative (No. 2016K1A4A4A01922028), the POSTECH BSRI Grant, and the KISTI supercomputing center (Grant No. KSC-2018-CRE-0064).

[1] D. Koskenmaki and K. A. Gschneidner, *Handbook on the Physics and Chemistry of Rare Earths* (Elsevier, Amsterdam, 1978), Chap. 4.

[2] J. C. Lashley, A. C. Lawson, J. C. Cooley, B. Mihaila, C. P. Opeil, L. Pham, W. L. Hults, J. L. Smith, G. M. Schmiedeshoff, F. R. Drymiotis, G. Chapline, S. Basu, and P. S. Riseborough, Tricritical Phenomena at the $\gamma \rightarrow \alpha$ Transition in $Ce_{0.9-x}La_xTh_{0.1}$ Alloys, Phys. Rev. Lett. **97**, 235701 (2006).

[3] N. Lanata, Y.-X. Yao, C.-Z. Wang, K.-M. Ho, J. Schmalian, K. Haule, and G. Kotliar, γ-α Isostructural Transition in Cerium, Phys. Rev. Lett. **111**, 196801 (2013).

[4] J. Wittig, Superconductivity of Cerium under Pressure, Phys. Rev. Lett. **21**, 1250 (1968).

[5] B. Johansson, The α-γ transition in cerium is a Mott transition, Philos. Mag. **30**, 469 (1974).

[6] J. W. Allen and R. M. Martin, Kondo Volume Collapse and the $\gamma \rightarrow \alpha$ Transition in Cerium, Phys. Rev. Lett. **49**, 1106 (1982).

[7] A. P. Murani, S. J. Levett, and J. W. Taylor, Magnetic Form Factor of α-Ce: Towards Understanding the Magnetism of Cerium, Phys. Rev. Lett. **95**, 256403 (2005).

[8] B. Chakrabarti, M. E. Pezzoli, G. Sordi, K. Haule, and G. Kotliar, α-γ transition in cerium: Magnetic form factor and dynamic magnetic susceptibility in dynamical mean-field theory, Phys. Rev. B **89**, 125113 (2014).

[9] K. Haule, V. Oudovenko, S. Y. Savrasov, and G. Kotliar, The $\alpha \rightarrow \gamma$ Transition in Ce: A Theoretical View from Optical Spectroscopy, Phys. Rev. Lett. **94**, 036401 (2005).

[10] K. Haule and T. Birol, Free Energy from Stationary Implementation of the DFT+DMFT Functional, Phys. Rev. Lett. **115**, 256402 (2015).

[11] M. Dzero, K. Sun, V. Galitski, and P. Coleman, Topological Kondo Insulators, Phys. Rev. Lett. **104**, 106408 (2010).

[12] M. Sundermann, F. Strigari, T. Willers, H. Winkler, A. Prokofiev, J. M. Ablett, J. P. Rueff, D. Schmitz, E. Weschke, M. Moretti Sala, A. Al-Zein, A. Tanaka, M. W. Haverkort, D. Kasinathan, L. H. Tjeng, S. Paschen, and A. Severing, $CeRu_4Sn_6$: A strongly correlated material with nontrivial topology, Sci. Rep. **5**, 17937 (2015).

[13] N. Wakeham, P. F. S. Rosa, Y. Q. Wang, M. Kang, Z. Fisk, F. Ronning, and J. D. Thompson, Low-temperature conducting state in two candidate topological Kondo insulators: SmB_6 and $Ce_3Bi_4Pt_3$, Phys. Rev. B **94**, 035127 (2016).

[14] F. Lu, J. Z. Zhao, H. Weng, Z. Fang, and X. Dai, Correlated Topological Insulators with Mixed Valence, Phys. Rev. Lett. **110**, 096401 (2013).

[15] M. Neupane, N. Alidoust, S. Y. Xu, T. Kondo, Y. Ishida, D. J. Kim, C. Liu, I. Belopolski, Y. J. Jo, T. R. Chang, H. T. Jeng, T. Durakiewicz, L. Balicas, H. Lin, A. Bansil, and S. Shin, Surface electronic structure of the topological Kondo-insulator candidate correlated electron system SmB_6, Nat. Commun. **4**, 2991 (2013).

[16] Z. Li, J. Li, P. Blaha, and N. Kioussis, Predicted topological phase transition in the SmS Kondo insulator under pressure, Phys. Rev. B **89**, 121117(R) (2014).

[17] K. Hagiwara, Y. Ohtsubo, M. Matsunami, S. Ideta, K. Tanaka, H. Miyazaki, J. E. Rault, P. L. Fèvre, F. Bertran, A. Taleb-Ibrahimi, R. Yukawa, M. Kobayashi, K. Horiba, H. Kumigashira, K. Sumida, T. Okuda, F. Iga, and S. Kimura, Surface Kondo effect and non-trivial metallic state of the Kondo insulator YbB_{12}, Nat. Commun. **7**, 12690 (2016).

[18] J. H. Shim, K. Haule, and G. Kotliar, Modeling the localized-to-itinerant electronic transition in the heavy fermion system $CeIrIn_5$, Science **318**, 1615 (2007).

[19] E. A. Goremychkin, H. Park, R. Osborn, S. Rosenkranz, J.-P. Castellan, V. R. Fanelli, A. D. Christianson, M. B. Stone, E. D. Bauer, K. J. McClellan, D. D. Byler, and J. M. Lawrence, Coherent band excitations in $CePd_3$: A comparison of neutron scattering and *ab initio* theory, Science **359**, 186 (2018).

[20] M. J. Lipp, D. Jackson, H. Cynn, C. Aracne, W. J. Evans, and A. K. McMahan, Thermal Signatures of the Kondo Volume Collapse in Cerium, Phys. Rev. Lett. **101**, 165703 (2008).

[21] See Supplemental Material at http://link.aps.org/supplemental/10.1103/PhysRevB.100.195138 for (i) computational details, (ii) phase boundaries, (iii) Lifshitz transition, (iv) topological phase transition above the critical point, (v) pressure-dependent DMFT physical quantities, (vi) TCI-type nature, and (vii) surface states at (111) surface of Ce, which includes Refs. [20,31,33–51].

[22] D. M. Wieliczka, C. G. Olson, and D. W. Lynch, High-resolution photoemission study of γ- and α-cerium, Phys. Rev. B **29**, 3028 (1984).

[23] F. Patthey, B. Delley, W.-D. Schneider, and Y. Baer, Low-Energy Excitations in α- and γ-Ce Observed by Photoemission, Phys. Rev. Lett. **55**, 1518 (1985).

[24] E. Weschke, C. Laubschat, T. Simmons, M. Domke, O. Strebel, and G. Kaindl, Surface and bulk electronic structure of Ce metal studied by high-resolution resonant photoemission, Phys. Rev. B **44**, 8304 (1991).

[25] Q. Y. Chen, W. Feng, D. H. Xie, X. C. Lai, X. G. Zhu, and L. Huang, Localized to itinerant transition of f electrons in ordered Ce films on W(110), Phys. Rev. B **97**, 155155 (2018).

[26] M. Grioni, P. Weibel, D. Malterre, Y. Baer, and L. Duo, Resonant inverse photoemission in cerium-based materials, Phys. Rev. B **55**, 2056 (1997).

[27] M. B. Zölfl, I. A. Nekrasov, Th. Pruschke, V. I. Anisimov, and J. Keller, Spectral and Magnetic Properties of α- and γ-Ce from Dynamical Mean-Field Theory and Local Density Approximation, Phys. Rev. Lett. **87**, 276403 (2001).

[28] K. Held, A. K. McMahan, and R. T. Scalettar, Cerium Volume Collapse: Results from the Merger of Dynamical Mean-Field Theory and Local Density Approximation, Phys. Rev. Lett. **87**, 276404 (2001).

[29] B. Amadon and A. Gerossier, Comparative analysis of models for the α-γ phase transition in cerium: A DFT+DMFT study using Wannier orbitals, Phys. Rev. B **91**, 161103(R) (2015).
[30] L. Huang and H. Lu, Electronic structure of cerium: A comprehensive first-principles study, Phys. Rev. B **99**, 045122 (2019).
[31] J. W. van der Eb, A. B. Kuz'menko, and D. van der Marel, Infrared and Optical Spectroscopy of α- and γ-Phase Cerium, Phys. Rev. Lett. **86**, 3407 (2001).
[32] Here, to capture the quasiparticle feature, the imaginary part of self-energy [Im $\Sigma(\omega)$] is set to be zero, namely, the Hamiltonian is assumed to be Hermitian.
[33] C.-J. Kang, H. C. Choi, K. Kim, and B. I. Min, Topological Properties and the Dynamical Crossover from Mixed-Valence to Kondo-Lattice Behavior in the Golden Phase of SmS, Phys. Rev. Lett. **114**, 166404 (2015).
[34] C.-J. Kang, D.-C. Ryu, J. Kim, K. Kim, J.-S. Kang, J. D. Denlinger, G. Kotliar, and B. I. Min, Multiple topological Dirac cones in a mixed-valent Kondo semimetal: *g*-SmS, Phys. Rev. Mater. **3**, 081201(R) (2019).
[35] K. Haule, C.-H. Yee, and K. Kim, Dynamical mean-field theory within the full-potential methods: Electronic structure of $CeIrIn_5$, $CeCoIn_5$, and $CeRhIn_5$, Phys. Rev. B **81**, 195107 (2010).
[36] B. Blaha, K. Schwarz, G. K. H. Madsen, D. Kvasnicka, and J. Luitz, *WIEN2k, An Augmented Plane Wave Plus Local Orbital Program for Calculating Crystal Properties* (Vienna University of Technology, Austria, 2001).
[37] K. Haule, Quantum Monte Carlo impurity solver for cluster dynamical mean-field theory and electronic structure calculations with adjustable cluster base, Phys. Rev. B **75**, 155113 (2007).
[38] P. Sémon, C. Yee, K. Haule, and A.-M. S. Tremblay, Lazy skip-lists: An algorithm for fast hybridization-expansion quantum Monte Carlo, Phys. Rev. B **90**, 075149 (2014).
[39] K. Haule, T. Birol, and G. Kotliar, Covalency in transition-metal oxides within all-electron dynamical mean-field theory, Phys. Rev. B **90**, 075136 (2014).
[40] A. A. Mostofi, J. R. Yates, Y.-S. Lee, I. Souza, D. Vanderbilt, and N. Marzari, Wannier90: A tool for obtaining maximally-localised Wannier functions, Comput. Phys. Commun. **178**, 685 (2008).
[41] J. Kuneš, R. Arita, P. Wissgott, A. Toschi, H. Ikeda, and K. Held, Wien2wannier: From linearized augmented plane waves to maximally localized Wannier functions, Comput. Phys. Commun. **181**, 1888 (2010).
[42] N. Marzari, A. A. Mostofi, J. R. Yates, I. Souza, and D. Vanderbilt, Maximally localized Wannier functions: Theory and applications. Rev. Mod. Phys. **84**, 1419 (2012).
[43] A. A. Mostofi, J. R. Yates, G. Pizzi, Y. S. Lee, I. Souza, D. Vanderbilt, and N. Marzari, An updated version of wannier90: A tool for obtaining maximally-localised Wannier functions, Comput. Phys. Commun. **185**, 2309 (2014).
[44] M. P. Lopez Sancho and J. M. Lopez Sancho, Highly convergent schemes for the calculation of bulk and surface Green functions, J. Phys. F: Met. Phys. **15**, 851 (1985).
[45] Q. S. Wu, S. N. Zhang, H.-F. Song, M. Troyer, and A. A. Soluyanov, WannierTools: An open-source software package for novel topological materials, Comput. Phys. Commun. **224**, 405 (2018).
[46] P. W. Bridgman, Rough compressions of 177 substances to 40,000 kg/cm^3, Proc. Am. Acad. Arts Sci. **76**, 71 (1948).
[47] A. W. Lawson and T.-Y. Tang, Concerning the High Pressure Allotropic Modification of Cerium, Phys. Rev. **76**, 301 (1949).
[48] L. H. Adams and B. L. Davis, Rapidly running transitions at high pressure. Proc. Nat. Acad. Sci. USA **48**, 982 (1962).
[49] B. J. Beaudry and P. E. Palmer, The lattice parameters of La, Ce, Pr, Nd, Sm, Eu and Yb, J. Less-Common Met. **34**, 225 (1974).
[50] I. M. Lifshitz, Anomalies of electron characteristics of a metal in the high pressure region, J. Exp. Theor. Phys. **11**, 1130 (1960).
[51] H. C. Choi, B. I. Min, J. H. Shim, K. Haule, and G. Kotliar, Temperature-Dependent Fermi Surface Evolution in Heavy Fermion $CeIrIn_5$, Phys. Rev. Lett. **108**, 016402 (2012).